Petroleum Science 23 (2026) 7282–7295

Contents lists available at ScienceDirect

Petroleum Science

journal homepage: www.keaipublishing.com/en/journals/petroleum-science

Original Paper

Investigation of secondary formation damage during hematite filter cake removal using acidic reducing systems in carbonate reservoirs

Amir Shokry [a], Salaheldin Elkatatny [a,*], Badr Bageri [b], Mustafa Al Ramadan [a]

[a] Department of Petroleum Engineering, King Fahd University of Petroleum & Minerals, Dhahran, 31261, Saudi Arabia
[b] Center for Integrative Petroleum Research, King Fahd University of Petroleum & Minerals, Dhahran, 31261, Saudi Arabia

ARTICLE INFO

Article history:
Received 9 November 2025
Received in revised form
2 February 2026
Accepted 1 June 2026
Available online 6 June 2026

Edited by Xi Zhang

Keywords:
Hematite
Filter cake
Acidic reducing systems
Secondary formation damage
Carbonate reservoirs
Iron precipitation

ABSTRACT

The removal of hematite-based filter cakes is essential to restore formation permeability after drilling operations. Although this process is commonly achieved using acidic systems, these fluids can induce secondary formation damage when interacting with carbonate formations. This study investigates the mechanisms and extent of such damage during the removal of hematite filter cakes using an acidic reducing system composed of hydrochloric acid (6 wt%) and ferrous chloride (10 wt%) under flowback and squeeze operational scenarios in carbonate formations. The experimental program was designed in two main phases to simulate field-relevant conditions and capture both the chemical and petrophysical aspects of secondary formation damage. In the first phase, hematite-saturated $FeCl_2$–HCl solutions were reacted with calcite powder to simulate fluid invasion into carbonate formations and to evaluate precipitation behavior and mineral type during acid neutralization. In the second phase, core-flooding experiments were performed using a modified setup on Indiana limestone plugs to assess the resulting damage under dynamic flow conditions. The workflow incorporated in-situ filter-cake buildup using a hematite-weighted drilling fluid, followed by treatment with the $FeCl_2$–HCl removal solution. Each core was characterized before and after treatment using computed tomography (CT) imaging, resistivity profiling, ultrasonic velocity measurements, and thin-section petrography. These integrated techniques enabled a comprehensive evaluation of secondary formation damage through the following indexes of permeability alteration, damage depth, and mechanical property changes under the two operational scenarios. The obtained results indicated that although the $FeCl_2$–HCl system effectively dissolved hematite, its interaction with carbonate minerals led to secondary precipitation of iron-bearing phases. XRD and SEM analyses confirmed the formation of siderite ($FeCO_3$) and magnetite (Fe_3O_4) as the dominant precipitates. Under the squeeze scenario, these iron-rich solids penetrated deeper into the carbonate matrix, causing almost 60% reduction in permeability and a marked increase in rock stiffness. In contrast, the flowback scenario confined precipitation to the near-wellbore region, limiting deep invasion and enabling partial restoration of permeability at the core face. This study demonstrates that acidic reducing systems, while effective for hematite dissolution, can induce significant secondary formation damage in carbonates due to redox-driven iron precipitation. The findings highlight the need to optimize acid formulations and operational strategies to preserve formation integrity during filter cake removal.

© 2026 The Authors. Publishing services by Elsevier B.V. on behalf of KeAi Communications Co. Ltd. This is an open access article under the CC BY license (http://creativecommons.org/licenses/by/4.0/).

1. Introduction

Drilling and completion operations in hydrocarbon reservoirs rely heavily on drilling fluids to maintain wellbore stability, control formation pressures, and facilitate cuttings transport to the surface (Basfar et al., 2025; Deville, 2022; Youssef et al., 2025). These fluids often operate in an overbalanced condition, where the hydrostatic pressure of the fluid exceeds that of the formation, inevitably leading to filtrate invasion and solid deposition on the formation face (Khatib, 1994; Louise et al., 2000). The deposition process forms a filter cake, a thin, low-permeability layer that restricts further fluid loss and stabilizes the borehole (Caenn et al., 2011). While this barrier is beneficial during drilling, it becomes a significant source

* Corresponding author.
E-mail address: elkatatny@kfupm.edu.sa (S. Elkatatny).
Peer review under the responsibility of China University of Petroleum (Beijing).

https://doi.org/10.1016/j.petsci.2026.06.001
1995-8226/© 2026 The Authors. Publishing services by Elsevier B.V. on behalf of KeAi Communications Co. Ltd. This is an open access article under the CC BY license (http://creativecommons.org/licenses/by/4.0/).

of productivity impairment if not efficiently removed prior to production. In open hole completions, the removal of the filter cake is essential to re-establish hydraulic communication between the wellbore and the reservoir and to avoid long-term permeability loss (Fink, 2021; Olivares et al., 2022).

Fig. 1 schematically illustrates the overall cycle from filter-cake formation during the drilling phase to its chemical dissolution during the cleanup stage, followed by the two possible operational approaches: squeeze and flowback scenarios. The figure provides a conceptual representation of how solids invasion leads to primary formation damage, and how the subsequent acid treatment can trigger secondary formation damage through secondary precipitation. This visual framework captures the entire life cycle of damage and treatment, emphasizing that the same process intended to restore formation permeability can, under certain conditions, create additional blockage or stiffness alteration deeper within the rock matrix.

1.1. Filter cake and primary formation damage

During drilling, the interaction between the invading filtrate and the rock matrix leads to primary formation damage, which is primarily mechanical in nature. This damage arises from the invasion of solids and the formation of the filter cake on the wellbore wall (Addagalla et al., 2016; Li and He, 2015). The solids within the drilling fluid-typically weighting materials, bridging agents, and clays - plug pore throats near the surface of the formation, reducing permeability in the invaded zone (Alotaibi et al., 2022; Mahmoud and Nasr-El-Din, 2021).

Among the commonly used weighting materials, hematite (Fe_2O_3) has gained increasing attention as an alternative to barite due to its higher specific gravity (~5.05 g/cm^3) and favorable rheological performance in high-density muds (Fadl et al., 2020; Osei, 2021). Hematite-weighted fluids produce thinner and more compact filter cakes, which are beneficial for wellbore stability (Bageri et al., 2021). However, hematite's higher hardness and its reactive iron oxide nature introduce challenges during removal (Tehrani et al., 2014).

The primary damage associated with hematite filter cake is therefore twofold: (1) physical plugging caused by fine solid invasion (Al Jaberi et al., 2024), and (2) the development of a low-permeability barrier that isolates the wellbore from the reservoir (Wang et al., 2015). Removing this cake requires an effective dissolution strategy that not only eliminates the solids but also avoids inducing further chemical damage during treatment (Fink, 2021).

1.2. Removal solution and secondary formation damage

The most common approach to remove hematite-based filter cakes is the use of strong mineral acids, particularly hydrochloric

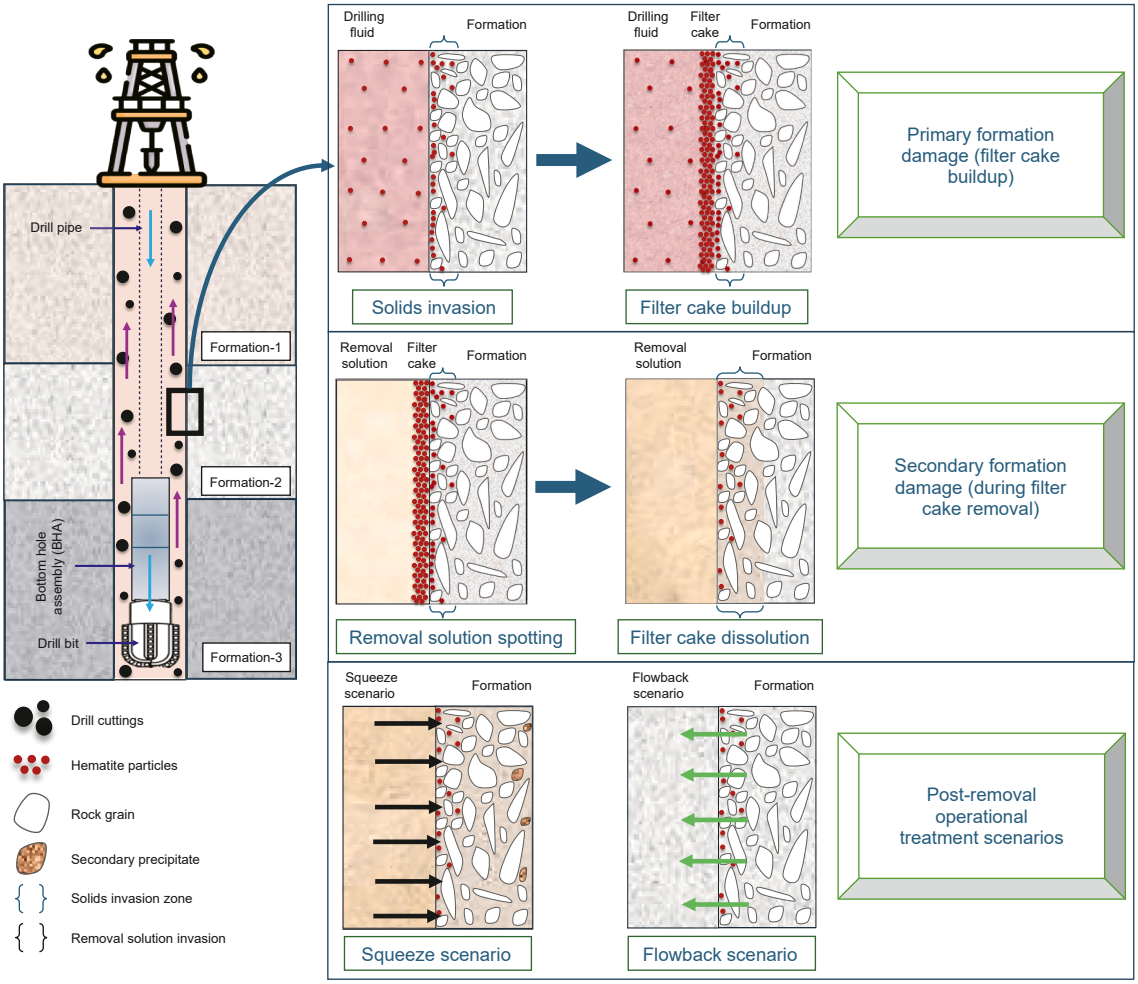


Fig. 1. Conceptual illustration of the sequence from filter-cake buildup to removal, showing flowback and squeeze scenarios and the transition from primary to secondary formation damage.

acid (HCl), which effectively dissolves iron oxides (Siddig et al., 2022). The dissolution reaction between hematite and HCl generates soluble ferric chloride ($FeCl_3$), allowing efficient oxide breakdown (Siddig et al., 2024). However, this process also produces ferric ions (Fe^{3+}), which are unstable under mildly acidic or near-neutral pH conditions (Gougler et al., 1985). As the acid becomes spent when reacting with carbonate rocks, the pH rises and Fe^{3+} ions hydrolyze and re-precipitate as insoluble phases such as iron hydroxides, oxides, and carbonates, leading to secondary formation damage (Shokry et al., 2025b; Shokry et al., 2026).

To improve dissolution kinetics and reduce the accumulation of ferric species, researchers have explored acidic reducing systems by incorporating electron-donating additives such as ferrous chloride ($FeCl_2$). The Fe^{2+} ions serve as reducing agents, converting Fe^{3+} to Fe^{2+} and maintaining iron in its soluble form. This mechanism significantly enhances hematite dissolution rates while mitigating corrosion compared to concentrated HCl (Siddig et al., 2024). However, when $FeCl_2$–HCl systems interact with carbonate formations, the rise in pH caused by calcite dissolution can trigger redox-driven iron precipitation, forming minerals such as siderite ($FeCO_3$) and magnetite (Fe_3O_4) (Shokry et al., 2025a). These secondary precipitates can invade the pore network, reduce permeability, and alter the mechanical integrity of the rock (Al Jaberi et al., 2021).

The dual chemical behavior of $FeCl_2$–HCl systems of rapid dissolution followed by precipitation introduces a complex interplay between fluid chemistry and rock reactivity, making it critical to evaluate their full impact on formation properties.

1.3. Operational scenarios: squeeze and flowback

After drilling, the removal stage begins once the drilling fluid is displaced by the selected removal solution. The treatment fluid is then allowed a defined soaking period to interact with the filter cake and initiate dissolution. During this period, the removal fluid progressively reacts with the filter cake and dissolve it (Abiodun et al., 2003; Rahmati et al., 2024).

If the filter cake is non-homogeneous as is typically the case along the openhole section, its thinner portions dissolve faster than the thicker segments (Al Otaibi et al., 2008). As a result, the removal solution in contact with these thinner areas becomes rapidly saturated with dissolved solids and can then invade slightly into the underlying formation (Bageri et al., 2023). This localized invasion occurs preferentially in zones where the filter cake has been fully or partially removed, allowing the spent fluid and its dissolved species to migrate a short distance into the pore system (Bageri et al., 2019). All of these interactions occur during the soaking period but once the soaking period is complete, the cleanup operation proceeds according to one of two main operational scenarios: flowback or squeeze (Fink, 2021).

In the flowback scenario, the well is opened to allow the formation to produce naturally, enabling the reverse flow of the treatment fluid and any entrained solids (Olubamise et al., 2014). This back-production helps remove any invaded or spent removal solution, along with secondary iron precipitates that may have formed as the pH increased during the reaction with carbonates (Zain and Sharma, 2001). The flowback process also assists in dislodging residual solids from the primary damage zone, thereby restoring near-wellbore permeability. Sufficient production time is typically maintained to ensure effective cleanup and removal of any accumulation caused by both primary and secondary mechanisms (Zain and Sharma, 1999).

The squeeze scenario, on the other hand, is applied when flowback is not feasible or not operationally desirable. This may occur in cases where well-control concerns restrict immediate production, when other completion operations (such as screen installation or packer setting) are planned, or when the well is designed for water injection rather than production (Nasr-El-Din, 2003). In such cases, the treatment fluid is injected into the formation under pressure and allowed to penetrate more deeply into the rock matrix. The squeeze approach promotes deep acid invasion, which can partially dissolve carbonate minerals, enhance rock properties, and help bypass the primary damage zone, particularly near the injection interval (Brady et al., 2000).

These two operational scenarios therefore represent contrasting cleanup strategies: the flowback mode focuses on near-wellbore cleaning and damage removal, while the squeeze mode emphasizes deeper acid penetration and potential stimulation (Willemse et al., 2005). However, the different fluid-flow patterns also mean that secondary iron precipitation and its associated damage may manifest differently in each case (Beall et al., 1996). Understanding these differences is essential for optimizing filter-cake removal operations using $FeCl_2$–HCl acidic reducing systems in carbonate formations.

Although previous studies have successfully optimized the $FeCl_2$–HCl acidic reducing system for hematite dissolution efficiency (Siddig et al., 2024) and characterized its precipitation behavior under static conditions (Shokry et al., 2025a), the extent to which secondary iron precipitation affects formation properties under dynamic flow conditions remains largely unexplored. Specifically, the influence of operational scenarios on the depth, magnitude, and nature of secondary formation damage in carbonate formations has not been established.

This research aims to bridge this gap by investigating the secondary formation damage tendency associated with $FeCl_2$–HCl acidic reducing systems during hematite filter-cake removal in carbonate rocks. The objectives of this study are to: (1) evaluate the precipitation mechanisms and identify the mineral phases formed during acid–carbonate interactions, (2) quantify the resulting changes in petrophysical and mechanical properties under different removal scenarios, and (3) compare the impact of flowback and squeeze operations, providing practical recommendations to minimize secondary formation damage during field applications.

2. Experimental methodology and workflow

Laboratory experiments were conducted under controlled conditions to evaluate secondary formation damage during hematite filter-cake removal using an $FeCl_2$–HCl acidic reducing system in carbonate rocks. The workflow involved filter-cake formation, acid treatment, and core-flooding tests simulating flowback and squeeze operations. Post-treatment characterization through CT imaging, permeability and resistivity measurements, mechanical testing, and petrography established the relationship between acid–rock interactions, iron precipitation, and the resulting changes in formation properties.

2.1. Fluid systems and core properties

2.1.1. Hematite–weighted drilling fluid

A hematite-weighted water-based drilling fluid was formulated to replicate field conditions and to build a representative filter cake across the core face under high-pressure/high-temperature (HPHT) conditions. The proposed fluid formulation, summarized in Table 1, was previously optimized by earlier researchers to minimize sag tendency and provide stable rheological and filtration properties under HPHT conditions (Ahmed et al., 2021).

2.1.2. $FeCl_2$–HCl acidic reducing system

The $FeCl_2$–HCl acidic reducing system was used as the main removal fluid to dissolve the hematite-based filter cake and evaluate secondary formation damage resulting from its interaction with carbonate rocks. This system combines the strong acidity of hydrochloric acid with the reducing capability of ferrous chloride, which stabilizes iron in the ferrous (Fe^{2+}) state and limits premature oxidation and ferric precipitation (Siddig et al., 2024).

The fluid was prepared by dissolving 10 wt% $FeCl_2$ in 6 wt% HCl under continuous stirring to ensure complete salt dissociation and minimize Fe^{2+} oxidation. The resulting solution had an initial pH of approximately 0.7 and remained chemically stable throughout preparation. To simulate field-relevant spent-acid conditions, the solution was subsequently pre-saturated with hematite by adding 10 g of hematite per 100 cm^3 of solution. The mixture was placed in a sealed aging cell and maintained in a hot-rolling oven at 250 °F for 24 h to ensure maximum hematite dissolution under high-temperature conditions. After aging, the solution was filtered to remove any undissolved solids, and the resulting clear hematite-saturated $FeCl_2$–HCl solution was used for the core-flooding experiments, representing the spent removal fluid expected during filter-cake cleanup.

2.1.3. Carbonate core properties and preparation

Homogeneous carbonate core plugs were prepared from Indiana limestone blocks to represent reservoir carbonate formations in the formation-damage assessment experiments. Indiana limestone was selected for its uniform mineralogy, moderate porosity, and predictable reactivity with acidic systems (Gomaa et al., 2018). Before testing, cores were oven-dried at 60 °C to constant weight, cooled to room temperature, and characterized for helium porosity, dry weight, dimensions, and liquid permeability using 3 wt % KCl brine to prevent clay swelling.

Two cores with comparable properties were prepared for each operational scenario (flowback and squeeze) to ensure reproducibility; one representative core from each scenario is presented. The baseline petrophysical properties are summarized in Table 2.

2.2. Reaction-induced precipitate characterization

Reaction tests were conducted to evaluate precipitation behavior and identify mineral phases formed during the interaction between the $FeCl_2$–HCl removal fluid and carbonate rock. Powdered calcite was added to a hematite-saturated $FeCl_2$–HCl solution at 250 °F to simulate removal-solution invasion into carbonate formations and to mimic fluid–rock interaction that leads to acid spending and pH increase under downhole conditions. This procedure was designed to represent spent-acid conditions expected during filter-cake cleanup in carbonate reservoirs. After completion of the reaction, the solution was filtered to collect the precipitated solids, which were then rinsed and dried at 60 °C prior to analysis. The recovered solids were analyzed using X-ray diffraction (XRD) and scanning electron microscopy (SEM) coupled with energy-dispersive X-ray spectroscopy (EDS) to determine mineralogy, morphology, and elemental composition. These analyses established the relationship between acid–carbonate reactions and secondary solid formation contributing to potential formation damage.

2.3. Core-flooding workflow and operational scenario simulation

A modified core-flooding system was used to enable both static filtration and dynamic flooding under controlled pressure and temperature conditions, simulating flowback and squeeze scenarios. The system was upgraded using corrosion-resistant stainless-steel fluid lines and fittings, with the line diameter increased from 1/8 inch to 1/4 inch to minimize the risk of plugging during solids-laden fluid injection, and was rated for operation up to 3000 psi and 300 °F. A hollow spacer was incorporated upstream of the core holder to provide a dedicated space for uniform in-situ filter-cake buildup across the core face, while facilitating solids transport during filtration. In addition, a ball-piston accumulator was used to maintain fluid homogenization prior to injection. Temperature during the core-flooding experiments was controlled using a heating oven, with the core holder and both fluid accumulators placed inside the oven to ensure uniform temperature distribution and representative thermal conditions along the entire flow path. The overall configuration of the modified setup is illustrated in Fig. 2.

2.3.1. Filter-cake buildup stage

The hematite-weighted drilling fluid formulated in Section 2.1.1 was used to form a representative hematite-based filter cake on the core inlet face using a procedure designed to mimic a standard HPHT filtration test, in which a filter paper or ceramic disk is typically employed. In this setup, the core face acted as the filtration medium, enabling in-situ filter-cake formation. The test began with a heating phase, during which the system was brought to 250 °F while the outlet valve was kept closed. After thermal stabilization, the outlet valve was opened, and the drilling fluid was injected in a single direction toward the core face under static filtration conditions at a constant differential pressure of 300 psi for 30 min. This stage simulated primary formation damage resulting from particle invasion and surface plugging.

Throughout the test, the injected fluid volume, filtrate volume, and filtration rate were continuously monitored and recorded to confirm uniform filter-cake deposition across the core surface. The filtrate volume was determined based on the reduction in the injection pump volume and the volume of effluent collected at the outlet. Because the core was initially fully saturated, the collected effluent represents the displacement of the in-situ pore fluid from the core rather than direct filtrate passing through the rock matrix.

Table 1
Composition and functional role of additives used in the hematite-weighted water-based drilling fluid formulated for filter cake buildup.

Additive	Primary function	Amount	Mixing time	Functional description
Base fluid	Continuous phase	245 cm^3	–	Provides water phase for hydration and dispersion of solids.
Defoamer	Antifoam agent	0.08 cm^3	1 min	Prevents foam generation during high-shear mixing.
Soda ash	Calcium ion control	0.5 g	1 min	Precipitates Ca^{2+} and stabilizes clay dispersion.
KOH	Alkalinity and pH controller	0.5 g	1 min	Adjusts pH and enhances additive hydration.
Bentonite	Viscosity builder	4 g	20 min	Improves gel strength and particle suspension.
Xanthan gum	Viscosity modifier	1.5 g	20 min	Enhances rheology and low-shear-rate viscosity.
Starch	Fluid-loss reducer	0.5 g	20 min	Decreases filtrate volume and improves filter-cake quality.
PAC-R	Fluid-loss and rheology control	1 g	20 min	Reduces filtrate loss and stabilizes rheology under HPHT conditions.
Hematite	Weighting material	350 g	10 min	Provides required mud density for wellbore pressure control.

Table 2
Baseline physical and petrophysical properties of the carbonate core samples.

Scenario	Core ID	Length, cm	Diameter, cm	Dry weight, g	Porosity, %	Liquid permeability, mD
Squeeze	S-1	97.95	38.12	250.76	17.9	72.5
Flowback	F-1	97.72	38.19	251.11	17.8	68.2

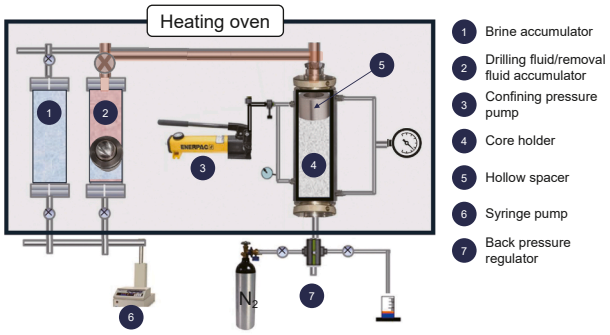


Fig. 2. Configuration of the upgraded core-flooding apparatus used in this study, illustrating the main modifications implemented to handle solids-laden drilling fluids and allow in-situ filter-cake formation.

2.3.2. Cake removal and fluid–rock interaction stage

After filtration, the core was removed, and the external filter cake was carefully scraped off. This step was intentionally performed to eliminate the influence of residual external filter-cake materials and to ensure that subsequent changes in petrophysical and mechanical properties could be directly attributed to fluid–rock interaction and secondary precipitation mechanisms, rather than incomplete cake dissolution or cake remnants penetrating the core. The core plug was then recharacterized to establish baseline properties before flooding. The hematite-saturated $FeCl_2$–HCl removal solution was injected using the same core-flooding setup described previously, under rate-controlled conditions at a constant flow rate of 0.5 cm^3/min, corresponding to 0.5 pore volume (PV), to simulate slow fluid invasion during field cleanup operations. During injection and soaking, the core was subjected to a confining pressure of 2000 psi, while a back pressure of 500 psi was maintained at the outlet to ensure stable single-phase flow conditions. Following injection, the core was sealed and soaked for 12 h at 250 °F to promote acid–rock interaction and potential iron re-precipitation, representing the early stage of secondary formation damage.

2.3.3. Post-treatment operational scenarios

Following the soaking period, two operational scenarios were simulated as presented in Fig. 1.

In the squeeze scenario, the reacted fluid (i.e., the hematite-saturated $FeCl_2$–HCl removal solution after soaking and reacting with the carbonate core) was re-injected at 0.5 cm^3/min into the downstream (second) half of the core, without reversing the flow direction. This configuration was selected to promote deeper fluid penetration beyond the near-wellbore region, simulating conditions where production is restricted or deeper acid penetration is required. This process allowed further invasion of the spent removal fluid into the carbonate matrix, increasing the likelihood of iron re-precipitation and the development of deeper secondary formation damage.

In the flowback scenario, brine was injected in the reverse-flow direction at the same flow rate to displace and produce back the reacted fluid, simulating natural production. This reverse flow enabled the removal of the reacted fluid and any entrained, mobile precipitates from the near-wellbore region, promoting localized cleanup, limiting deep fluid invasion, and enabling partial restoration of permeability.

2.4. Core characterization and damage evaluation techniques

Each core was characterized at multiple stages to track changes in petrophysical and mechanical properties throughout the experiments. Baseline measurements were obtained before treatment, followed by evaluation after filter-cake buildup to quantify primary damage and after flowback or squeeze tests to assess secondary formation damage caused by the $FeCl_2$–HCl system.

After each scenario, the cores were cut into near-wellbore and deep sections to examine damage distribution. Permeability, CT imaging, and resistivity measurements were used to identify dissolution and precipitation features and to locate conductive iron-rich zones. Ultrasonic tests provided compressional (Vp) and shear (Vs) velocities for calculating Young's modulus and Poisson's ratio using standard ultrasonic pulse velocity (UPV) equations based on Vp, Vs, and bulk density, following the ASTM standard method (Gamal et al., 2020). These parameters were used to evaluate stiffness and elasticity changes. Thin-section petrography further confirmed mineralogical alterations, pore plugging, and textural modification.

This work is intended as a mechanistic study to investigate secondary formation damage processes associated with $FeCl_2$–HCl filter-cake removal under different operational scenarios. Therefore, the results are presented as representative observations obtained under controlled laboratory conditions, rather than as a statistically comprehensive assessment. The overall experimental workflow adopted in this study is summarized in Fig. 3.

3. Results and discussions

This section presents and discusses the main findings obtained from the experimental program, linking the chemical reaction behavior of the $FeCl_2$–HCl removal system with the resulting petrophysical and mechanical alterations in carbonate cores. The final part provides a comparative analysis of these scenarios, highlighting their distinct impacts on formation properties and offering operational recommendations for mitigating secondary formation damage during field-scale filter-cake removal.

3.1. Precipitation behavior and mineral phase identification

Powdered calcite was gradually added to the hematite-saturated $FeCl_2$–HCl solution in incremental stages until the solution pH increased from its initial value of 0.7 to about 4.0. A total of 16 g of calcite per 100 cm^3 of solution was required to reach this condition. As the reaction progressed, the initially transparent reddish solution became darker and noticeably more viscous, indicating the onset of secondary solid formation. After 2 h of reaction, the precipitate was collected, washed, and dried for characterization. The total recovered solid mass was approximately 12 g per 100 cm^3 of reacted solution.

The XRD analysis (Fig. 4) confirmed that the precipitates were dominated by magnetite (Fe_3O_4), accounting for roughly two-

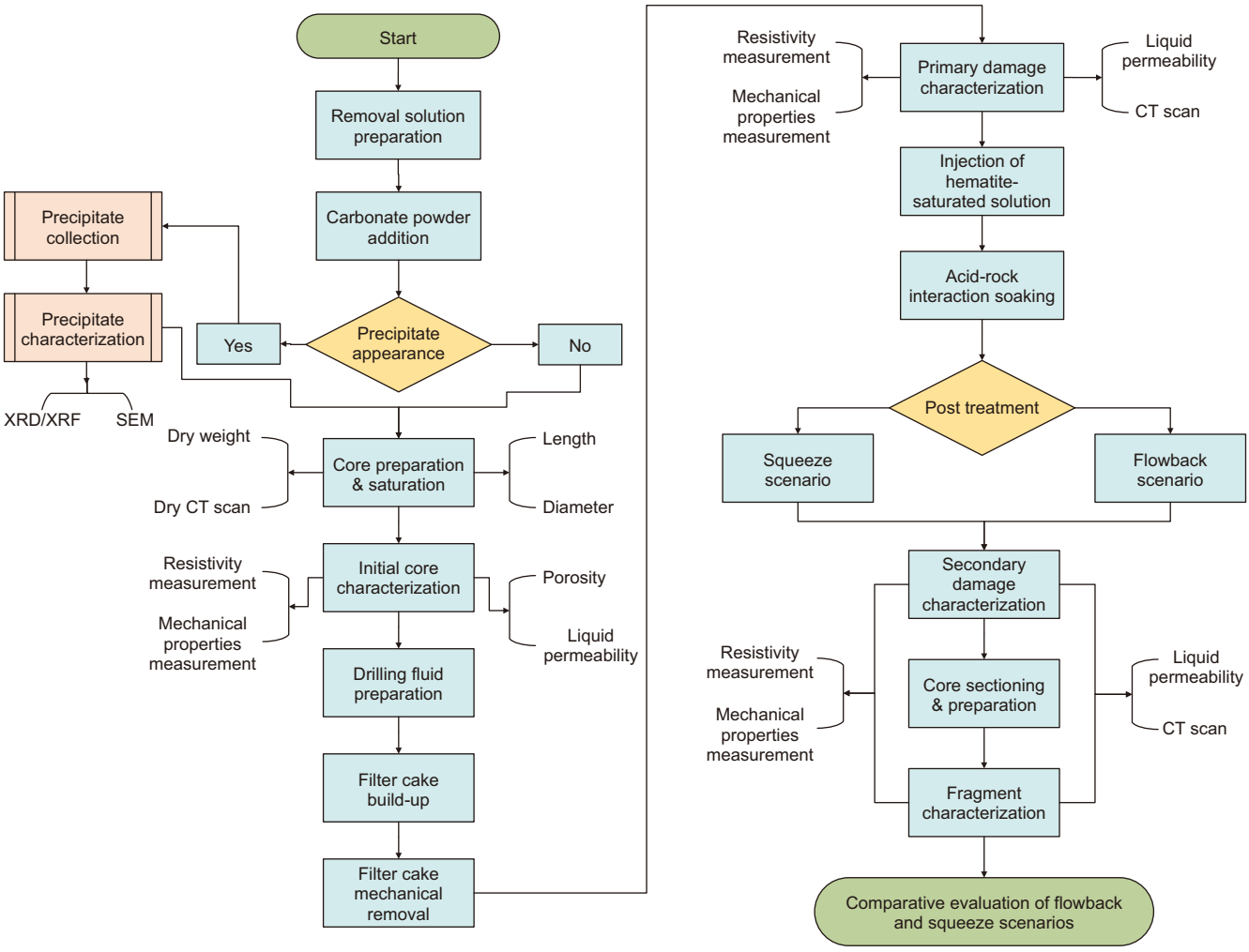


Fig. 3. Experimental workflow for filter-cake removal and post-treatment evaluation under squeeze and flowback scenarios.

thirds of the total solid, with siderite ($FeCO_3$) representing the remaining one-third. Characteristic diffraction peaks of magnetite appeared at 2θ values near 30.1°, 35.5°, 43.2°, and 62.9°, while siderite peaks were observed at 24.0°, 32.0°, 37.0°, and 51.0°. The relative peak intensities suggest that magnetite was the dominant crystalline phase.

SEM imaging (Fig. 5) revealed aggregates of fine sub-micron magnetite particles intergrown with rhombohedral siderite crystals, forming dense clusters that could readily obstruct pore throats if deposited within a porous medium. The rhombohedral siderite crystals are highlighted by green arrows in Fig. 5(a), while the fine magnetite grains appear to coat or cement the coarser siderite crystals, consistent with a sequential precipitation process.

The observed mineral assemblage can be explained by the coupled acid–carbonate–iron redox reactions occurring during the pH increase. Initially, hematite (Fe_2O_3) dissolution in the $FeCl_2$–HCl medium produces Fe^{2+} ions under strongly acidic and reducing conditions (Siddig et al., 2024):

$$Fe_2O_3 + 6\,HCl \rightarrow 2FeCl_3 + 3H_2O \quad (1)$$

As the acid reacts with calcite ($CaCO_3$), CO_2 is released and the solution pH gradually rises. This neutralization process consumes H^+ and promotes hydrolysis and oxidation of Fe^{2+}, leading to the nucleation of magnetite. Simultaneously, dissolved CO_2 equilibrates with the solution to form bicarbonate and carbonate species that react with residual Fe^{2+} to produce siderite according to:

$$Fe^{2+} + CO_3^{2-} \rightarrow FeCO_3\ (s) \quad (2)$$

At early stages, when pH < 2 and Fe^{2+} dominates, small clusters of Fe_3O_4 form through internal electron exchange between Fe^{2+} and Fe^{3+}. As the pH approaches 4, carbonate activity increases, stabilizing siderite as a secondary phase. The coexistence of magnetite and siderite therefore reflects a transition from redox-controlled precipitation (Fe^{2+}/Fe^{3+} exchange) to carbonate-complexation-driven precipitation as acidity decreases.

From a formation-damage perspective, this mineralogical evolution is critical. The fine magnetite particles are likely to migrate and deposit deeper within pore networks under squeeze conditions, creating low-permeability zones, whereas the rhombohedral siderite crystals tend to accumulate near the rock surface or within larger pores. Together, these phases can substantially reduce permeability and alter mechanical stiffness by cementing the pore structure. These findings confirm that pH evolution during acid–carbonate interaction can transform a chemically benign reducing system into a source of secondary iron-bearing solids responsible for secondary formation damage.

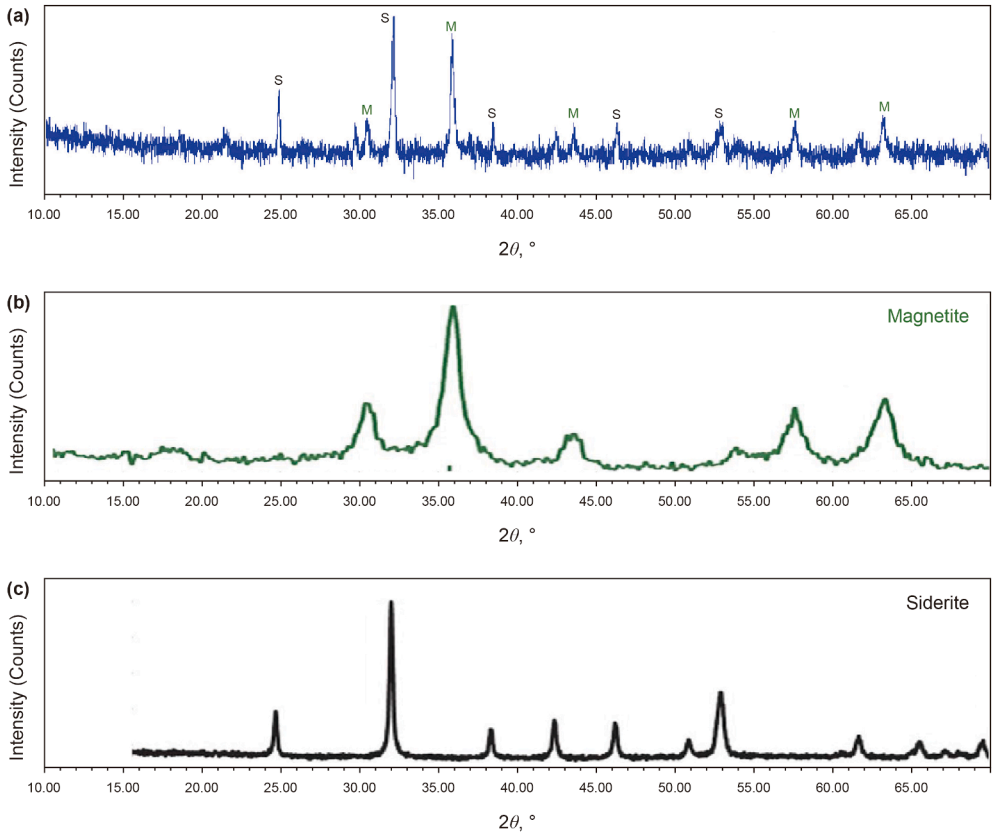


Fig. 4. XRD patterns showing (**a**) iron-bearing precipitates formed during $FeCl_2$–HCl–carbonate interaction, (**b**) reference pattern for magnetite (Fe_3O_4) (Jamshidiyan et al., 2017), and (**c**) reference pattern for siderite ($FeCO_3$) (Holme et al., 2023).

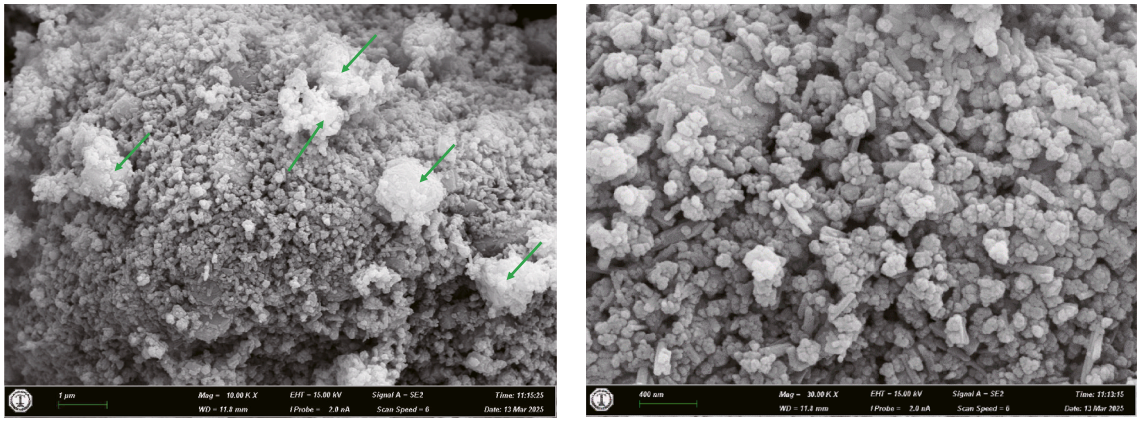


Fig. 5. SEM images of magnetite and siderite precipitates formed from the $FeCl_2$–HCl carbonate reaction at 250 °F (left: 1 μm; right: 400 nm).

3.2. Post-treatment operational scenarios

3.2.1. Squeeze post-treatment scenario

During the primary-damage stage, static filtration across the core face at a differential pressure of 300 psi and temperature of 250 °F was conducted for 30 min to generate a representative hematite-based filter cake. The cumulative filtrate volume increased rapidly during the initial spurt-loss period and then stabilized at approximately 9 cm^3 after 25 min, as shown in Fig. 6(a). The plateau in filtrate volume during the final 5 min of the test indicates that the cake had become effectively impermeable, fully sealing the core surface and preventing further fluid invasion. The resulting cake formed a uniform, cohesive layer with an average thickness of 3/32 inch, as illustrated in Fig. 6(b). After the test, the external filter cake was carefully removed to expose the underlying core surface (Fig. 6(c)). The image clearly shows that some fine solids remained embedded within the pore openings, confirming that solid invasion occurred during filtration and that the internal portion of the cake persisted within the rock matrix. This residual internal damage represents the baseline primary formation damage before the squeeze treatment with the $FeCl_2$–HCl removal solution.

The CT-scan profile of core S-1 (Fig. 7) provides a clear visualization of the density variation along the core length before and

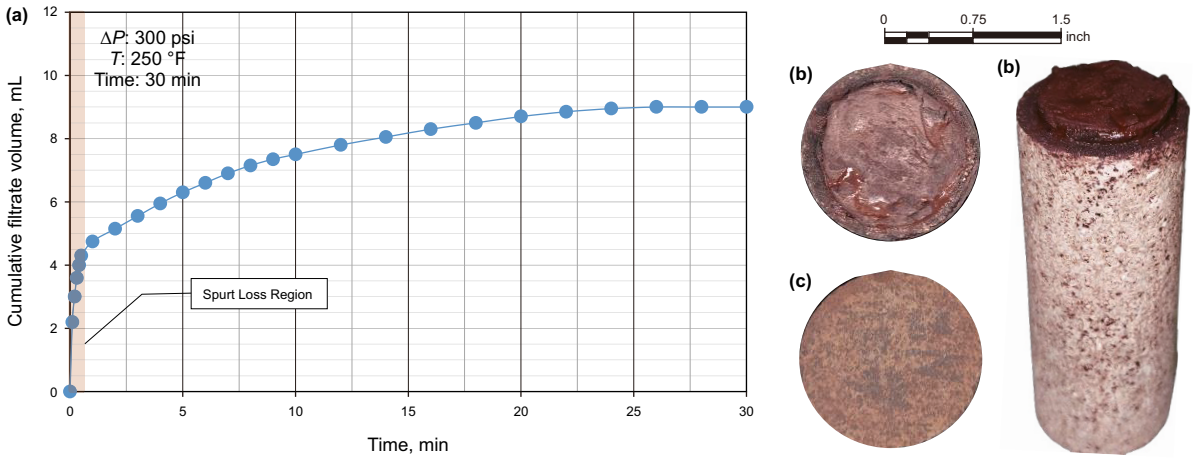


Fig. 6. Filtration results for hematite-weighted drilling fluid across core S-1 showing (**a**) filtrate volume profile, (**b**) cohesive filter-cake layer, and (**c**) residual solids after cake removal indicating pore invasion.

after treatment. The reference curve (blue line) represents the undamaged carbonate baseline, while the post-cake formation profile (red line) shows a noticeable rise in CT number near the inlet region (0–15 mm), indicating particle invasion and surface plugging due to hematite deposition during static filtration. This localized densification marks the primary formation-damage zone, where fine solids infiltrated the pore throats and reduced local porosity.

After the squeeze treatment with the $FeCl_2$–HCl removal solution, the post-squeeze profile (black line) revealed two distinct behaviors. In the inlet region, the CT number dropped below the primary-damage level, reflecting net dissolution of carbonate minerals during the 12-h soaking stage. The acid–rock reaction partially offset the effect of the previously invaded solids, indicating that chemical dissolution exceeded the mass of retained filter-cake particles or any newly formed precipitates in that near-surface zone. Despite the persistence of primary damage features, the reduction in CT number demonstrates that matrix dissolution dominated this section of the core.

Further along the core (60–80 mm from the inlet), the CT number increased markedly, forming the secondary formation damage zone. This densification indicates the deep invasion and precipitation of iron-bearing solids, mainly magnetite and siderite, transported during the squeeze process. These deposits accumulated in the deeper pore network, confirming that while the squeeze treatment effectively removed the filter cake, it also promoted secondary precipitation deeper within the formation. The combined CT evidence shows a transition from mechanically

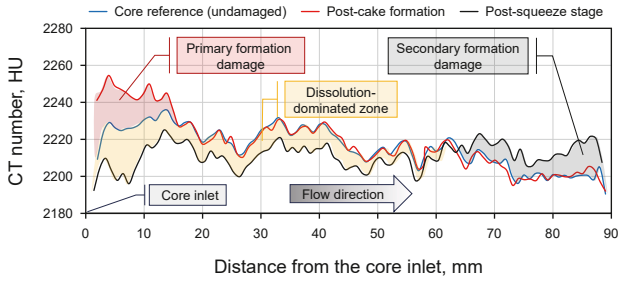


Fig. 7. CT-scan profile of core S-1 showing CT-number variation along the flow direction. The curves compare the core reference, post-cake formation, and post-squeeze stages, highlighting densification near the inlet due to solids invasion and iron-precipitate accumulation.

induced near-surface damage to chemically driven deep damage, consistent with the mineralogical findings and permeability trends discussed in subsequent sections.

It should be noted that CT imaging provides information on relative density variations rather than direct mineral identification. Therefore, changes in CT number observed in this study are interpreted as indicators of bulk density alteration within the core, which may result from a combination of secondary precipitation, dissolution residues, or solid redistribution. The interpretation of CT-number increases as precipitation-dominated zones is supported by independent evidence from XRD, SEM/EDS, permeability, resistivity, and mechanical property measurements, rather than relying on CT data alone.

The permeability measurements for the core subjected to the squeeze treatment are presented in Fig. 8(a). The initial (undamaged) permeability of the 4-in. core was 72.5 mD, which declined sharply to 28.2 mD after filter-cake formation due to pore plugging and solid invasion at the surface. Following exposure to the $FeCl_2$–HCl removal solution during the squeeze stage, the overall permeability increased to 58.8 mD, indicating partial recovery as a result of acid-induced dissolution near the inlet region.

After this test, the core was sectioned into two equal halves to assess the spatial distribution of damage. The first half (near-wellbore region) exhibited a marked permeability enhancement to 88.7 mD, consistent with the CT observations that showed reduced CT numbers near the inlet, where acid–rock dissolution exceeded the retained solids or secondary precipitates. In contrast, the second half (far-zone region) displayed a significant permeability reduction to 41.9 mD, confirming the development of secondary formation damage through deep precipitation of iron-bearing minerals transported during the squeeze process. These results demonstrate that, while the squeeze operation restored permeability near the wellbore, it simultaneously induced damage deeper in the formation which is a clear manifestation of the dual nature of the squeeze treatment.

The electrical resistivity of core S-1, measured using two- and four-pole configurations (Fig. 8(b)), consistently decreased with progressive formation damage. The undamaged core showed the highest resistivity (≈8.4 and 8.2 Ω·m), reflecting the clean carbonate matrix. After filter-cake formation, values dropped to 7.5 and 7.1 Ω·m due to hematite invasion and conductive layer buildup. Following the squeeze treatment, resistivity declined further to about 5.3 and 5.2 Ω·m, attributed to the combined effect of iron-rich, electrically conductive precipitates and acid–rock

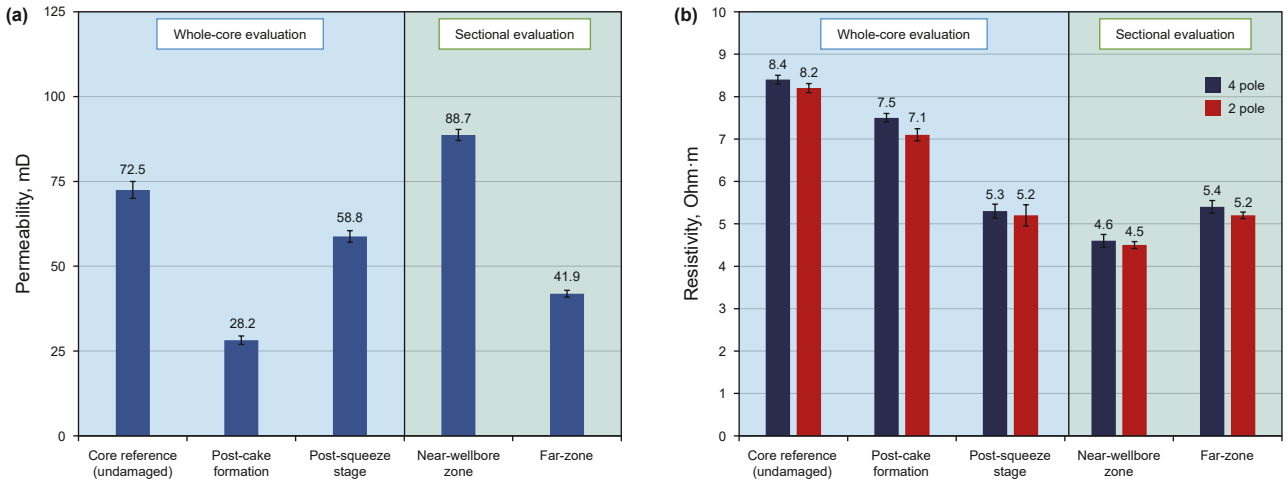


Fig. 8. Permeability and resistivity of core S-1 during squeeze treatment: (**a**) permeability recovery near the wellbore and decline in the far zone; (**b**) resistivity decrease due to hematite invasion, iron precipitation, and acid–rock dissolution.

dissolution, which enhanced conductivity through both the pore fluid and the solid matrix.

Sectional analysis showed lower resistivity near the wellbore (≈4.6 Ω·m) compared to the far zone (≈5.3 Ω·m), consistent with partial pore occupation by conductive iron precipitates that did not completely block fluid pathways, allowing continuous ionic transport through the remaining pore fluid. Overall, the resistivity trends reflect the combined effects of solids invasion, conductive iron precipitation, and carbonate dissolution during the squeeze treatment, resulting in enhanced conductivity rather than resistivity increase.

The mechanical properties of the core before and after the squeeze treatment were evaluated in terms of Young's modulus and Poisson's ratio, as shown in Fig. 9. The undamaged core exhibited a Young's modulus of 35.6 GPa and a Poisson's ratio of 0.38, characteristic of an intact carbonate matrix with well-connected pores. Following filter-cake formation, the Young's modulus increased to 43.6 GPa, while the Poisson's ratio decreased to 0.29, indicating a stiffer and less ductile rock framework. This change reflects the infilling of pore spaces by hematite particles, which restricts elastic deformation and enhances the overall stiffness of the composite matrix, a behavior that can adversely affect near-wellbore deformability and reduce the rock's ability to accommodate stress changes during production or injection.

After exposure to the $FeCl_2$–HCl removal solution during the squeeze stage, the modulus slightly decreased to 38.5 GPa, while the Poisson's ratio increased marginally to 0.32. This shift suggests that acid-induced dissolution near the inlet partially counteracted the stiffening effect of the solids invasion, restoring some flexibility to the rock framework. From an engineering perspective, this localized softening may improve pore connectivity and short-term flow capacity near the wellbore, but the values remained above the original state, confirming that residual solids and secondary iron precipitates continued to influence the mechanical response.

When the treated core was sectioned for zonal analysis, the near-wellbore section exhibited the lowest modulus (33.6 GPa) and the highest Poisson's ratio (0.33), consistent with the dissolution-dominated region observed in CT and permeability analyses. In contrast, the far-zone section displayed a higher modulus (41.5 GPa) and a lower Poisson's ratio (0.30), confirming that secondary precipitation of magnetite and siderite within the deeper formation increased stiffness and reduced deformability. Such stiffness increase in the far zone may hinder elastic deformation, contribute to permeability impairment, and negatively impact long-term injectivity or productivity. These mechanical results reinforce the dual impact of the squeeze treatment, acid dissolution near the inlet and iron precipitation in the deeper zone, which together define the contrasting mechanical behavior along the core length and highlight the importance of controlling fluid invasion depth to balance cleanup efficiency and mechanical integrity.

The thin-section micrographs presented in Fig. 10 provide direct petrographic evidence of the contrasting alteration mechanisms across the core after the squeeze treatment. The reference sample, prepared from the same carbonate block prior to testing, shows a clean, well-connected pore network filled with blue epoxy and minimal mineral alteration, reflecting the pristine state of the rock. In comparison, the near-wellbore section (Fig. 10(a)) exhibits extensive acid-induced dissolution, producing irregular and enlarged pore spaces that confirm intense rock–fluid interaction. However, fine residual iron-rich precipitates remain trapped within smaller pores, indicating that although significant dissolution occurred, the squeeze operation did not completely clean the invaded zone. This observation is consistent with the permeability enhancement and CT-scan density reduction observed in this region. The dissolution pathways are clearly visible, indicating that acid–rock interaction dominated the damage evolution near the inlet.

In contrast, the far-zone section (Fig. 10(b)) displays partially plugged pores and limited evidence of additional dissolution. The pore size distribution remains nearly unchanged relative to the pre-treatment state, suggesting that the acid was largely consumed during the initial near-wellbore reaction and lost its dissolution capacity deeper in the core. Consequently, the spent fluid transported and deposited iron-bearing precipitates, primarily magnetite and siderite, into the far-zone pores, creating a secondary precipitation zone that restricted flow pathways. These microstructural observations confirm that the squeeze process produced two distinct alteration regimes: a dissolution-dominated but partially cleaned near-wellbore zone, and a precipitation-dominated far zone formed after acid neutralization and iron transport. This dual behavior is consistent with the petrophysical, and CT evidence discussed earlier.

3.2.2. *Flowback scenario*

During the primary-damage stage of the flowback test, static filtration was performed at a differential pressure of 300 psi and a

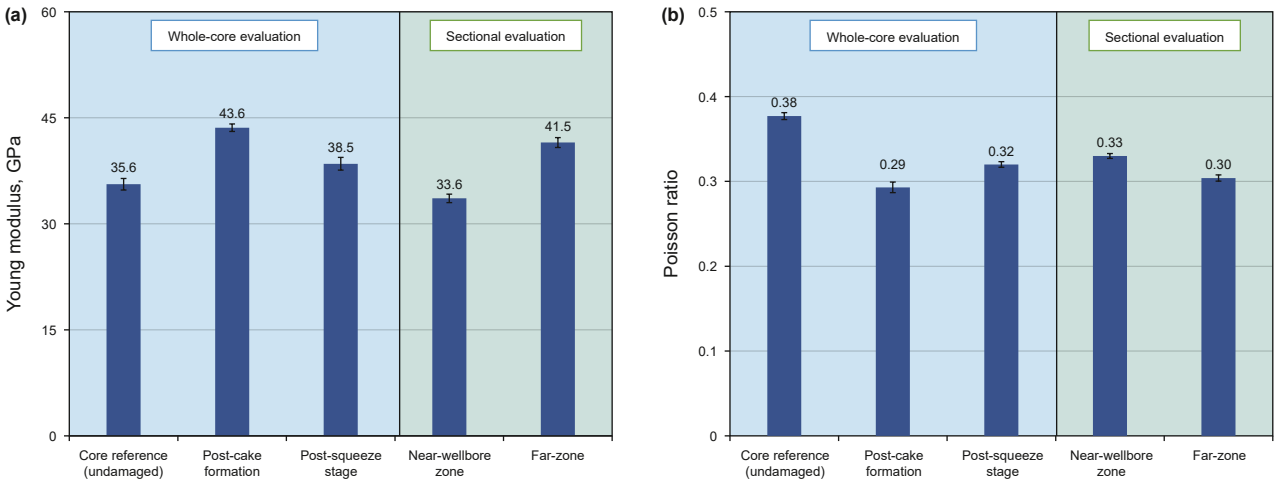


Fig. 9. Mechanical properties of core S-1 during squeeze treatment showing increased stiffness after solids invasion and reduced ductility near the wellbore due to dissolution.

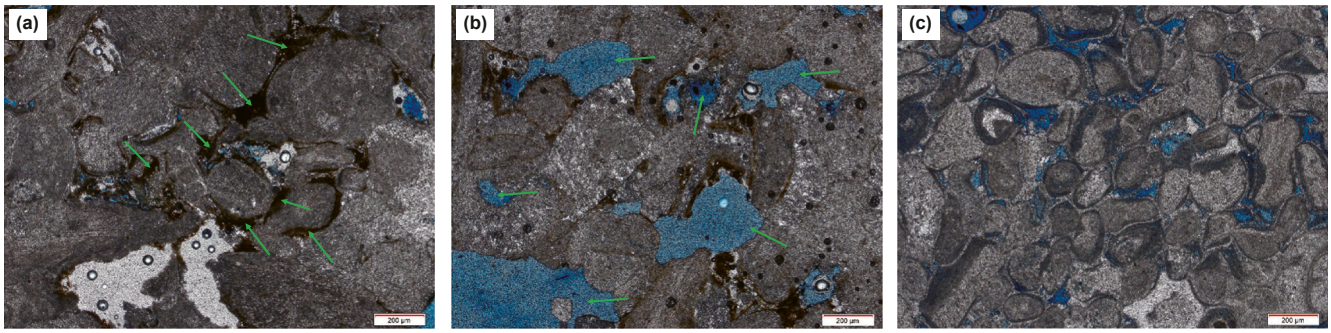


Fig. 10. Thin-section micrographs of core S-1 after squeeze treatment (200 μm): (**a**) near-wellbore dissolution; (**b**) far-zone pore plugging by iron precipitates; (**c**) reference sample with unaltered carbonate texture.

temperature of 250 °F for 30 min to develop a representative hematite-based filter cake. The cumulative filtrate profile (Fig. 11(a)) shows a rapid increase during the initial spurt-loss period, followed by gradual stabilization at a total volume of 8.5 cm^3 over the final 6 min of the test. This plateau indicates that the cake had become effectively impermeable, forming a sealing layer that prevented further filtrate passage through the core. The resulting filter cake exhibited a uniform, cohesive texture with an average thickness of 3/32 inch, as shown in Fig. 11(b).

After filtration, the external filter cake was carefully removed to prepare the surface for the subsequent flowback stage (Fig. 11(c)). However, the cleaned surface still displayed fine reddish-brown solids embedded within the pore openings, representing the internal filter cake formed by hematite particles and drilling-fluid fines that penetrated the shallow pore structure during static filtration. This internal residue confirms that even after external cake removal, a portion of the invaded solids remained integrated with the rock matrix, reducing permeability and connectivity within the near-surface region. The persistence of this internal damage establishes the baseline condition of the core prior to the flowback treatment, where the $FeCl_2$–HCl removal solution was subsequently applied to evaluate its secondary formation damage tendency.

The CT-scan profile of the core subjected to the flowback treatment (Fig. 12) illustrates the evolution of density distribution along the flow direction before and after the cleanup process. The reference curve (blue line) represents the undamaged carbonate matrix, while the post-cake formation profile (red line) shows an elevated CT number within the first 15 mm from the inlet, corresponding to the primary damage zone formed by hematite particle invasion and solids deposition during filtration.

Following the flowback operation, the post-flowback curve (black line) exhibits a marked decrease in CT number across the near-inlet region compared to the post-cake condition. This reduction indicates partial dissolution of the invaded solids and the underlying carbonate rock, which enhanced porosity and reduced bulk density. This area, identified as the dissolution-dominated zone, where the $FeCl_2$–HCl solution effectively removed internal filter-cake residues and re-opened previously blocked pore pathways.

Unlike the squeeze scenario, the flowback treatment did not promote deeper precipitation or secondary formation damage; instead, the CT number gradually converged toward the baseline beyond 50 mm, showing that precipitates and dissolved materials were effectively flushed out rather than transported deeper into the formation. The overall CT profile confirms that the flowback operation successfully limited deep fluid invasion, achieving localized cleaning near the wellbore and mitigating the risk of secondary formation damage.

The permeability measurements for the flowback scenario are shown in Fig. 13(a), highlighting the improvement in flow capacity following the removal treatment. The initial (undamaged) core exhibited a permeability of 68.2 mD, which decreased sharply to 31.3 mD after filter-cake formation, reflecting pore blocking and solid invasion during static filtration. After exposure to the $FeCl_2$–HCl solution under flowback conditions, the whole-core

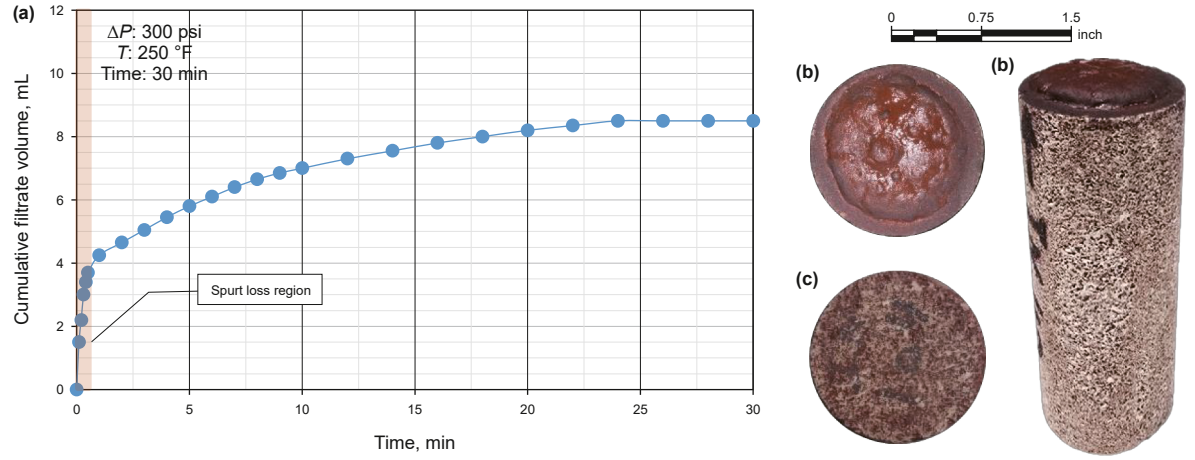


Fig. 11. Filtration results for hematite-weighted drilling fluid across core F-1 showing (**a**) filtrate volume profile, (**b**) cohesive filter-cake layer, and (**c**) residual solids after cake removal indicating pore invasion.

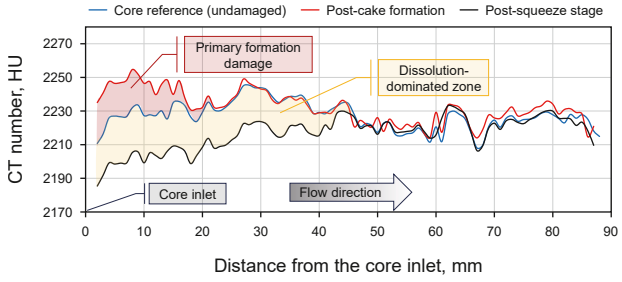


Fig. 12. CT-scan profile of core F-1 after flowback showing primary damage near the inlet and a dissolution-dominated zone where acid–rock interaction removed residues, improving porosity.

permeability increased to 73.6 mD, surpassing the original value, indicating effective removal of internal filter-cake residues and acid-induced matrix dissolution that enhanced pore connectivity.

To evaluate the spatial variation, the treated core was sectioned into near-wellbore and far-zone halves. The near-wellbore section recorded the highest permeability of 84.6 mD, confirming the dominance of dissolution and the partial removal of embedded solids in this region. In contrast, the far-zone section exhibited a permeability of 65.2 mD, which is nearly comparable to the original core. This consistency suggests that the flowback operation remained localized, as the reactive fluid did not significantly invade the second half of the core. The limited fluid penetration prevented further dissolution or secondary precipitation, confirming that the flowback process efficiently cleaned the near-wellbore region without extending deep into the formation or inducing secondary formation damage.

Fig. 13(b) shows the electrical resistivity of core F-1 measured using two- and four-pole configurations. The reference core exhibited the highest resistivity (≈8.1 and 7.9 Ω·m), which decreased to 7.3 and 7.0 Ω·m after filter-cake formation due to conductive hematite and drilling-fluid fines. Following the flowback treatment, resistivity further declined to about 6.0 Ω·m, reflecting the combined effects of acid-induced dissolution, which enhanced pore connectivity, and limited iron precipitation introducing minor conductive phases.

Sectional analysis confirmed this behavior: near-wellbore resistivity (≈5.5 Ω·m) was lower than the far-zone values, consistent with localized dissolution and minimal deep invasion. The absence of significant conductive precipitates in the far zone indicates that flowback confined chemical reactions to the near-wellbore region, achieving effective cleanup without deep formation alteration.

The mechanical properties of the core under the flowback scenario are presented in Fig. 14, showing variations in Young's modulus and Poisson's ratio for both whole-core and sectional evaluations. The reference core exhibited a Young's modulus of 36.3 GPa and a Poisson's ratio of 0.34. Following filter-cake formation, the Young's modulus increased to 43.1 GPa, while the Poisson's ratio decreased to 0.30, indicating a stiffer and less ductile framework due to the infilling of pores with hematite particles and drilling-fluid solids.

After the flowback treatment, the overall Young's modulus decreased to 33.5 GPa, accompanied by an increase in Poisson's ratio to 0.36, suggesting that acid–rock dissolution restored some pore volume and reduced stiffness in the rock matrix. From an engineering perspective, this mechanical softening near the wellbore can enhance pore connectivity and improve cleanup efficiency and short-term productivity. When the treated core was divided into sections, the near-wellbore zone exhibited the lowest modulus (31.3 GPa) and the highest Poisson's ratio (0.37), consistent with a dissolution-dominated region where the acid fluid enhanced porosity and weakened the rock framework.

Conversely, the far-zone section displayed a higher modulus (37.7 GPa) and a lower Poisson's ratio (0.34), reflecting limited fluid invasion and the preservation of the original rock integrity. Maintaining mechanical stability in the far zone is advantageous from a completion and reservoir management perspective, as it minimizes the risk of unintended formation weakening or permeability alteration away from the wellbore. These results confirm that the flowback operation led to localized dissolution and mechanical softening near the inlet, while maintaining the mechanical stability of the deeper formation, thereby offering a more favorable balance between effective cleanup and preservation of formation integrity in contrast to the squeeze scenario that induced deeper stiffening from secondary precipitation.

The thin-section micrographs presented in Fig. 15 confirm the localized effect of the flowback treatment on the pore structure of the carbonate core. The reference sample (Fig. 15(c)) shows clean, well-connected intergranular pores filled with blue epoxy, representing the undamaged matrix prior to any treatment. The first half of the treated core (Fig. 15(a)) reveals extensive acid-induced dissolution, characterized by enlarged and irregular pore boundaries with no visible residual solids or iron precipitates. Even the smaller pore throats appear open and free of fines, confirming that

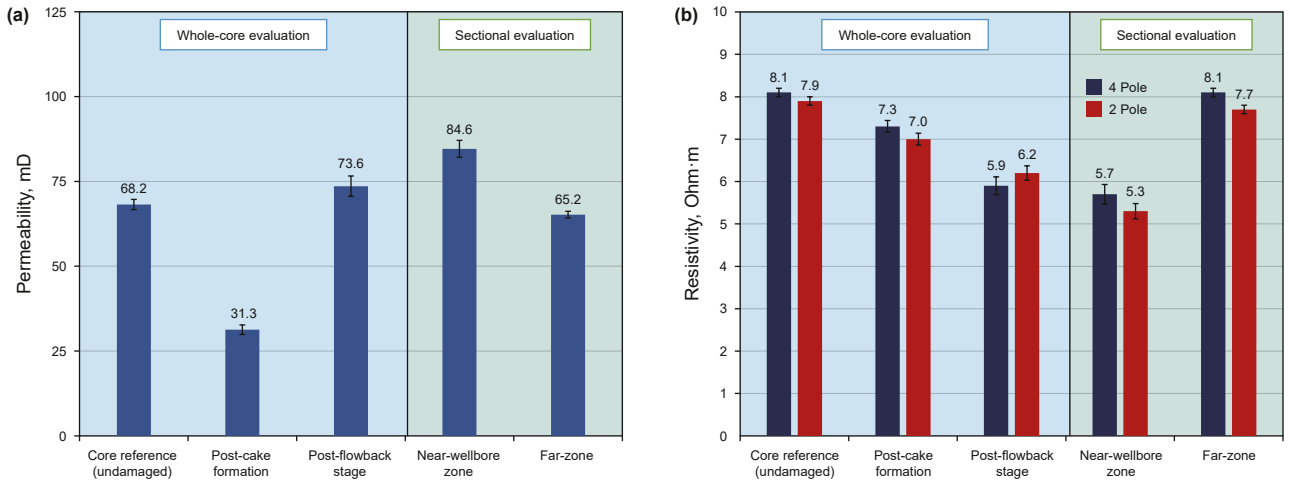


Fig. 13. Permeability and resistivity of core F-1 during flowback treatment: (**a**) permeability increase near the wellbore and stability in the far zone; (**b**) resistivity trends indicating localized dissolution near the inlet and limited deep invasion.

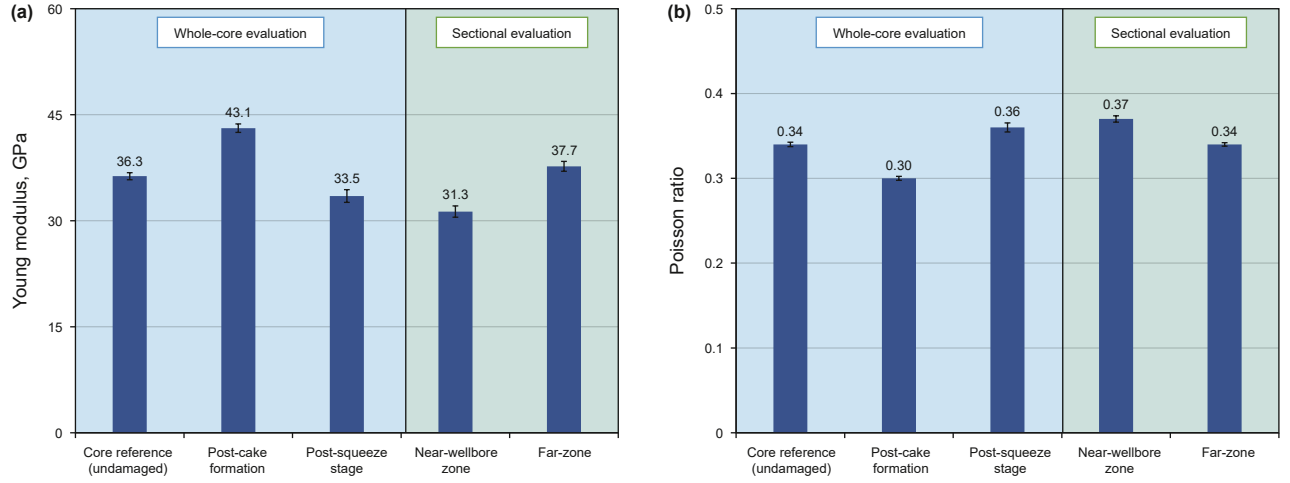


Fig. 14. Mechanical properties of core F-1 during flowback treatment showing decreased stiffness and increased ductility near the wellbore due to acid-induced dissolution.

the flowback operation efficiently removed the internal filter-cake residues and fully restored pore connectivity near the wellbore.

The second half of the core (Fig. 15(b)) exhibits a microstructure similar to the reference sample, with limited dissolution and no evidence of secondary precipitation. The pore geometry in this section remains largely unaltered, indicating that the reactive fluid did not invade the far zone and that the acid spent its reactivity near the inlet during the flowback phase. These petrographic observations demonstrate that the flowback treatment achieved complete cleaning and dissolution in the near-wellbore region while maintaining the original pore structure in the deeper section, thereby avoiding secondary formation damage.

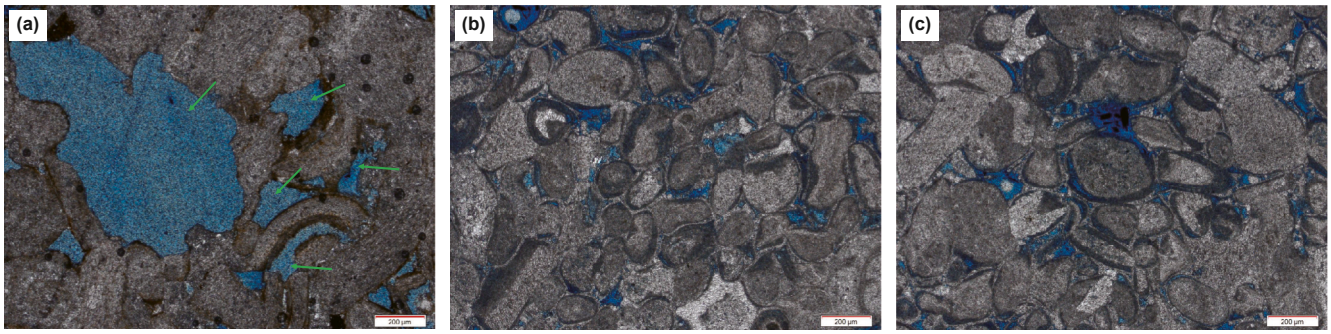


Fig. 15. Thin-section micrographs of core F-1 after flowback treatment (200 μm): (**a**) near-wellbore dissolution with clean, open pores; (**b**) far-zone with minimal alteration; (**c**) reference sample showing unaltered carbonate texture.

3.3. Comparative analysis of operational scenarios and recommendations

A comparative evaluation of the squeeze and flowback scenarios highlights the distinct damage mechanisms and cleanup performance of the $FeCl_2$–HCl reducing system during hematite filter-cake removal. Although both scenarios used the same formulation, differences in flow direction, injected volume, and fluid residence time produced contrasting effects on formation properties.

In the squeeze scenario, deep fluid penetration and prolonged interaction promoted complete external filter-cake dissolution but also caused re-precipitation of iron-bearing minerals (magnetite and siderite) within the carbonate matrix. CT and permeability data revealed a secondary formation damage zone in the deeper core section, where permeability dropped by about 50%. Resistivity decreased due to conductive precipitates, while mechanical tests showed increased stiffness and reduced ductility. Thin-section analysis confirmed pore plugging by iron-rich deposits, evidencing chemically induced deep damage under the specific squeeze conditions evaluated in this study.

In contrast, the flowback scenario promoted localized dissolution and limited invasion. CT scans showed near-wellbore density reduction without deep alteration. Permeability exceeded the original value, and resistivity decreased due to improved pore connectivity. Mechanical data indicated local softening near the inlet, and petrography confirmed clean, open pores with unaltered structure in the far zone. Under the tested conditions, flowback provided effective cleaning and permeability recovery while minimizing the risk of deep secondary precipitation.

It should be emphasized that the comparative outcomes presented here are condition-dependent. The primary objective of this study is to demonstrate the tendency for secondary formation damage associated with the $FeCl_2$–HCl system and to provide a comparative evaluation of squeeze and flowback operational scenarios based on the resulting petrophysical and mechanical property changes. The effectiveness of squeeze operations is strongly influenced by operational parameters such as injected volume, soaking (dwell) time, and timing of backflow, which control the extent of fluid invasion, acid spending, and secondary iron precipitation. While the squeeze scenario exhibited a higher risk of secondary damage under the conditions tested, appropriate optimization of these controlling parameters may mitigate deep formation damage and improve squeeze performance, representing an important direction for future research.

From an operational perspective, several key recommendations can be drawn:

- For carbonate reservoirs with hematite-based filter cakes, flowback operations are favorable under conditions where near-wellbore cleanup and minimal deep invasion are desired and should be optimized to promote efficient flushing while limiting reaction time to minimize iron re-precipitation.
- Introducing iron-sequestering or complexing agents into the $FeCl_2$–HCl system may help stabilize iron ions during the pH rise, reducing the risk of secondary precipitation under squeeze conditions; however, such formulations must first demonstrate effective hematite filter-cake dissolution.
- The squeeze method should be applied with caution and appropriate operational control and is best suited for removal fluids that do not introduce secondary formation damage tendency, while flowback remains a robust option for standard cleanup operations under the tested conditions.

4. Conclusions

This study investigated the tendency for secondary formation damage associated with using an $FeCl_2$–HCl acidic reducing system for the removal of hematite-based filter cakes in carbonate formations. The work combined chemical precipitation analysis, core-flooding experiments, and multi-scale characterization techniques, including CT scanning, resistivity profiling, mechanical testing, and thin-section petrography, to evaluate two operational scenarios: squeeze and flowback. The comparative results provide new insights into the dissolution–precipitation dynamics of the system and their implications for formation integrity under the experimental conditions investigated.

The following key conclusions can be drawn:

- The $FeCl_2$–HCl system efficiently dissolves hematite; however, when reacting with carbonates, it generates iron-rich secondary precipitates (magnetite and siderite) as the pH increases, representing a potential source of secondary formation damage.
- Under squeeze conditions, as applied in this study, deep acid penetration and prolonged fluid residence time promoted secondary precipitation within the carbonate matrix, resulting in substantial permeability reduction (up to 60%), resistivity decrease, and increased rock stiffness due to pore infilling by iron minerals.
- CT and petrographic analyses confirmed two distinct alteration regimes during squeeze treatments: (1) a dissolution-dominated near-wellbore zone and (2) a precipitation-dominated far zone.
- The flowback scenario confined the reaction to the near-wellbore region, where acid–rock dissolution dominated, leading to permeability recovery exceeding the original value and complete cleaning of the internal filter cake without inducing deep precipitation under the tested conditions.

Overall, the results indicate that flowback operations are more favorable under the specific experimental conditions evaluated in this work, as they promote near-wellbore restoration while minimizing the risk of deep secondary formation damage. The effectiveness of squeeze treatments, however, is strongly dependent on operational parameters such as injected volume, dwell time, and backflow timing, and may be improved through appropriate optimization.

CRediT authorship contribution statement

Amir Shokry: Writing – original draft, Methodology, Investigation, Formal analysis, Conceptualization. **Salaheldin Elkatatny:** Writing – review & editing, Visualization, Supervision, Methodology, Investigation, Conceptualization. **Badr Bageri:** Writing – review & editing, Visualization, Validation, Methodology, Conceptualization. **Mustafa Al Ramadan:** Writing – review & editing, Visualization, Validation, Investigation.

Declaration

The authors affirm that this study was performed independently and that no financial or personal conflicts of interest have influenced the research process or the conclusions drawn.

Funding

The authors declare that no external financial support was provided for this research by public, commercial, or non-profit entities.

Declaration of competing interest

The authors declare that they have no known competing financial interests or personal relationships that could have appeared to influence the work reported in this paper.

Acknowledgements

The authors gratefully acknowledge King Fahd University of Petroleum and Minerals (KFUPM), Dhahran, Saudi Arabia, for providing the laboratory facilities and technical support required to complete this work. The authors also extend their appreciation to Badr Eldin Petroleum Company for granting A.S. a study leave to pursue and conduct this research.

References

Abiodun, A., Nwabueze, V., Opusunju, A., et al., 2003. Successful application of mud cake pop-off technique in horizontal well bore cleanup - case histories. In: SPE European Formation Damage Conference, Richardson. Society of Petroleum Engineers, p. SPE 82277. https://doi.org/10.2118/82277-ms.

Addagalla, A.K., Kosandar, B.A., Lawal, I.G., et al., 2016. Overcoming OBM filter cake damage using micro-emulsion remediation technology across a high-temperature formation. In: SPE International Conference and Exhibition on Formation Damage Control, Richardson. Society of Petroleum Engineers, p. SPE 178942. https://doi.org/10.2118/178942-ms.

Ahmed, A., Basfar, S., Solling, T.I., et al., 2021. Prevention of hematite settling in water-based mud at high pressure and high temperature. ACS Omega 6 (36), 23607–23613. https://doi.org/10.1021/acsomega.1c03818.

Al Jaberi, J., Bageri, B.S., Adebayo, A.R., et al., 2021. Evaluation of formation damages during filter cake deposition and removal process: The effect of primary damage on secondary damage. Pet. Sci. 18 (4), 1153–1162. https://doi.org/10.1016/j.petsci.2021.07.004.

Al Jaberi, J., Bageri, B., Otain, W., et al., 2024. Fine-tuning filter cake sealing performance: The role of particle size in hematite weighted water-based drilling fluid. ACS Omega 9 (23), 25084–25093. https://doi.org/10.1021/acsomega.4c02352.

Al Otaibi, M.B., Nasr-El-Din, H.A., Hill, A.D., 2008. Characteristics and removal of filter cake formed by formate-based drilling mud. In: SPE International Symposium and Exhibition on Formation Damage Control, Richardson. Society of Petroleum Engineers, p. SPE 112427. https://doi.org/10.2118/112427-ms.

Alotaibi, N., Lawson-Jack, A., Smith, K., et al., 2022. Damage mechanism of high-density Mn_3O_4/$BaSO_4$ based workover fluids in carbonate reservoirs. In: International Petroleum Technology Conference. IPTC. https://doi.org/10.2523/iptc-22033-ea.

Bageri, B.S., Adebayo, A.R., Barri, A., et al., 2019. Evaluation of secondary formation damage caused by the interaction of chelated barite with formation rocks during filter cake removal. J. Petrol. Sci. Eng. 183, 106395. https://doi.org/10.1016/j.petrol.2019.106395.

Bageri, B.S., Gamal, H., Elkatatny, S., et al., 2021. Effect of different weighting agents on drilling fluids and filter cake properties in sandstone formations. ACS Omega 6 (24), 16176–16186. https://doi.org/10.1021/acsomega.1c02129.

Bageri, B., Al Jaberi, J., Adebayo, A.R., et al., 2023. Understanding the complexity of secondary formation damage: mechanism and detection strategies during filter cake removal process. Geoenergy Sci. Eng. 231, 212287. https://doi.org/10.1016/j.geoen.2023.212287.

Basfar, S., Shokry, A., et al., 2025. Evaluation of the effects of Kaolin clay on the performance of barite-weighted oil-based drilling fluid. ACS Omega 10 (10), 9976–9985. https://doi.org/10.1021/acsomega.4c07376.

Beall, B.B., Brannon, H.D., TjonJoePin, R.M., et al., 1996. Evaluation of a new technique for removing horizontal wellbore damage attributable to drill-In filter cake. In: SPE Annual Technical Conference and Exhibition, Richardson. Society of Petroleum Engineers, p. SPE 36429. https://doi.org/10.2118/36429-ms.

Brady, M.E., Ali, S.A., Price-Smith, C., et al., 2000. Near wellbore cleanup in open-hole horizontal sand control completions: laboratory experiments. In: SPE International Symposium on Formation Damage Control, Richardson. Society of Petroleum Engineers, p. SPE 58785. https://doi.org/10.2118/58785-ms.

Caenn, R., Darley, H.C.H., Gray, G.R., 2011. The filtration properties of drilling fluids. In: Composition and Properties of Drilling and Completion Fluids. Elsevier, Amsterdam, pp. 271–306. https://doi.org/10.1016/b978-0-12-383858-2.00006-8.

Deville, J., 2022. Drilling Fluids, pp. 115–185.

Fadl, A.M., Abdou, M.I., El-Sayed Ahmed, H., et al., 2020. Delaminated iron ore (hematite-barite) as alternative weighting agent to barite in petroleum drilling fluids engineering operations and mechanism study. Ain Shams Eng. J. 11 (4), 1317–1337. https://doi.org/10.1016/j.asej.2020.03.005.

Fink, J., 2021. Filter Cake Removal, pp. 419–439.

Gamal, H., Elkatatny, S., Abdulraheem, A., et al., 2020. Exposure time impact on the geomechanical characteristics of sandstone formation during horizontal drilling. Molecules 25 (11), 2480. https://doi.org/10.3390/molecules25112480.

Gomaa, A.M., Nino-Penaloza, A., Cutler, J., et al., 2018. Insights of wormhole propagation during carbonate acidizing: a comparison between constant injection pressure versus constant volumetric rate. J. Energy Resour. Technol. 140 (10), 102906. https://doi.org/10.1115/1.4039443.

Gougler, P.D., Coulter, A.W., Hendrick, J.E., 1985. Field Investigation Identifies Source and Magnitude of Iron Problems. https://doi.org/10.2118/13812-MS.

Holme, E.A., Henkes, G.A., Tosca, N.J., et al., 2023. Experimental constraints on siderite clumped isotope thermometry. Geochem. Cosmochim. Acta 343, 323–340. https://doi.org/10.1016/j.gca.2022.12.012.

Jamshidiyan, M., Shirani, A.S., Alahyarizadeh, G., 2017. Solvothermal synthesis and characterization of magnetic Fe_3O_4 nanoparticle by different sodium salt sources. Mater. Sci. Pol. 35 (1), 50–57. https://doi.org/10.1515/msp-2017-0004.

Khatib, Z.I., 1994. Prediction of formation damage due to suspended solids: modeling approach of filter cake buildup in injectors. In: SPE Annual Technical Conference and Exhibition, Richardson. Society of Petroleum Engineers, p. SPE 28488. https://doi.org/10.2118/28488-ms.

Li, D., He, W., 2015. Journey into filter cakes: a microstructural study. In: International Petroleum Technology Conference. IPTC. https://doi.org/10.2523/iptc-18246-ms.

Louise, B., Boek, E., Jacques, S., et al., 2000. Particulate invasion from drilling fluids. SPE Journal 5, 412–419. https://doi.org/10.2118/67853-PA.

Mahmoud, O., Nasr-El-Din, H.A., 2021. Formation-damage assessment and filter-cake characterization of Ca-bentonite fluids enhanced with nanoparticles. SPE Drill. Complet. 36 (1), 75–87. https://doi.org/10.2118/191155-pa.

Nasr-El-Din, H.A., 2003. New mechanisms of formation damage: lab studies and case histories. In: SPE European Formation Damage Conference, Richardson. Society of Petroleum Engineers, p. SPE 82253. https://doi.org/10.2118/82253-ms.

Olivares, T.D., Al-Zahrani, W., Latter, K., et al., 2022. Nano technology micro-emulsion technology removed invert emulsion fluid filter cake damage after delayed action across sandstone reservoir. In: ADIPEC, Richardson: Society of Petroleum Engineers, p. SPE 211496. https://doi.org/10.2118/211496-ms.

Olubamise, T.O., Oghene, U.J., Uchendu, C., 2014. Maximising well productivity through appropriate design of cleanup recipe and proper execution for new well completions. In: SPE Nigeria Annual International Conference and Exhibition, Richardson. Society of Petroleum Engineers, p. SPE 172457. https://doi.org/10.2118/172457-ms.

Osei, H., 2021. Comparative analysis of the effect of barite and hematite on the rheology of water-based drilling mud. Trends Petrol. Eng. 1 (2). https://doi.org/10.53902/tpe.2021.01.000508.

Rahmati, M., Khosravi, M., Tanha, A.A., et al., 2024. Evaluation of formation damage and filter cake removal with a new LPM drilling fluid additive. Results Eng. 23, 102656. https://doi.org/10.1016/j.rineng.2024.102656.

Shokry, A., Bageri, B., Elkatatny, S., 2025a. Damage tendency of HCl-based solutions during hematite-based filter-cake removal in carbonate formations. SPE J. 30 (9), 5402–5417. https://doi.org/10.2118/228408-pa.

Shokry, A., Elkatatny, S., Bageri, B., et al., 2025b. Iron precipitation and secondary plugging during acid removal of hematite-based filter cakes. In: Middle East Oil, Gas and Geosciences Show (MEOS GEO), Richardson. Society of Petroleum Engineers, p. SPE 227485. https://doi.org/10.2118/227485-ms.

Shokry, A., Elkatatny, S., Bageri, B., 2026. Formation damage assessment in carbonate reservoirs after removing hematite-water-based filter cake using HCl. Sci. Rep. 16, 192. https://doi.org/10.1038/s41598-025-29161-5.

Siddig, O., Alafnan, S., Elkatatny, S., 2022. Removal of hematite water-based filter cake using hydrochloric acid. Geofluids, 4924465. https://doi.org/10.1155/2022/4924465.

Siddig, O., Elkatatny, S., Alafnan, S., 2024. Optimizing hematite filter cake treatment using reducing agents. Sci. Rep. 14, 11857. https://doi.org/10.1038/s41598-024-62746-0.

Tehrani, A., Cliffe, A., Hodder, M.H., et al., 2014. Alternative drilling fluid weighting agents: a comprehensive study on ilmenite and hematite. In: IADC/SPE Drilling Conference and Exhibition, Richardson. Society of Petroleum Engineers, p. SPE 167937. https://doi.org/10.2118/167937-ms.

Wang, J.B., Mo, J., Xiong, Y., et al., 2015. Effect of composition of drilling fluid on filter cake shear strength. Drill. Fluid Complet. Fluid 32 (3), 65–69. https://doi.org/10.3969/j.issn.1001-5620.2015.03.018 (in Chinese).

Willemse, M., Mostafa, O., El-Ashry, M., et al., 2005. Ensuring effective stimulation treatments in difficult completionsPaper presented at the SPE/ICoTA Coiled Tubing Conference and Exhibition, The Woodlands. Texa. https://doi.org/10.2118/93987-MS.

Youssef, A.S., Mahmoud, A.A., Elkatatny, S., et al., 2025. A review of the critical conditions required for effective hole cleaning while horizontal drilling. Petroleum 11 (2), 143–157. https://doi.org/10.1016/j.petlm.2025.02.002.

Zain, Z.M., Sharma, M.M., 1999. Cleanup of wall-building Filter Cakes, p. SPE-56635. https://doi.org/10.2118/56635-MS.

Zain, Z.M., Sharma, M.M., 2001. Mechanisms of mudcake removal during flowback. SPE Drill. Complet. 16 (4), 214–220. https://doi.org/10.2118/74972-pa.